International Journal of Civil Engineering

Geotechnical Engineering

Drained and undrained sand behaviour by multilaminate bounding surface model

Seyed Amirodin Sadrnejad*, Hamid Karimpour

Received: July 2009, Revised: January 2010, Accepted: May 2010

Abstract

The present paper is devoted to a new critical state based plasticity model able to predict drained and undrained behaviour of granular material. It incorporates a bounding surface plasticity model describing in multilaminate framework to capitalize on advantages of this mathematical framework. Most of the models developed using stress/strain invariants are not capable of identifying the parameters depending on directional effects such as principal stress rotation and fabric; this is mainly because stress/strain invariants are scalar quantities. The principal features of this model can be postulated as considering both inherent and induced anisotropy, principal stress rotation. Since the local instability of saturated sand within post-liquefaction is highly dependent on the residual inherent/induced anisotropy, bedding plane effects and also the stress/strain path the new mode is competent to be employed in this regard. The constitutive equations of the model are derived within the context of non-linear elastic behaviour for the whole medium and plastic sliding of interfaces of predefined planes. As follows, the constitutive equations are described in detail and then the experimental results and sensitive analysis of key material constants are shown which all imply the power of the model in predicting of soil behaviour under any condition in soil structures.

Keywords: Multilaminate, Elastic-plastic, Bounding surface, Drained, Undrained

1. Introduction

A numerous number of constitutive models have been presented with different capabilities, mostly based on experimental observations of material behavior and on a framework of elasticity and plasticity theories. However, based on various conditions and types of soils including grading, soil texture, presence of water, loading condition and etc there are rooms to progress. Samples of the classic capable models in literature are Drucker et al. [1], Roscoe and Burland [2], DiMaggio and Sandler [3], Lade [4], Prevost [5], Mroz et al. [6], Ghaboussi and Momen [7], Desai and Faruque [8], Poorooshasb and Pietruszak [9], Dafalias and Herrmann [10], Frantziskonis et al. [11], and Crouch et al. [12].

Furthermore, Taylor [13] first presented a framework called Multilaminate. Multilaminate framework is semi-micromechanical tool based on obtaining the numerical integration between inter granular behaviors, and mechanical properties in the form of a constitutive law. In other words, in this framework material properties stem from properties of each component; therefore, achievement to stress-strain behavior of soils is possible by surveying inter granular displacements. Multilaminate framework can not predict the behavior of material independently, and it must be declared in the form of a constitutive law. This constitutive law obtains the treatment of each plane. By using this framework the overall behavior is, therefore, acquired by accumulating behaviors of all defined planes. In this way, there are no limitations to choose the constitutive law. Batdrof and Budiansky [14] described a plasticity theory in this framework for metals. It stated that sliding in material in any direction develops some shear plastic strain which is related to the shear stress path components. Zienkiewicz and Pande [15] utilized this framework and expanded to rocks. A similar approach was, also, employed by Pande and Piretruszczak [16] and Pande and Sharma [17] to predict liquefaction of layered sand called reflecting surface model and clays behaviour, respectively. Bazant and Oh [18] declared a new model, called micro-plane, using an identical theory for analyzing cracking in concrete.

It sometimes seems that by blending or individualizing some rules it is possible to overcome some of difficulties and propose some new techniques to clarify vague points of

* *Corresponding Author: sadrnejad@kntu.ac.ir*
1 Dept. of Civil Eng, K.N.Toosi University of Tech., Teheran, Iran
2 Dept. of Civil Eng, the Catholic University of America., Washington, DC, USA

problems. Due to the abilities of the Multilaminate framework, a constitutive model, named Unified 3D Critical State Bounding-Surface model for Soils Incorporating Continuous Plastic Loading under Cyclic Paths proposed by Crouch et al. [12] is employed to be explained in this framework, and present a new elastoplastic model with more abilities. It should be noted that the mentioned constitutive formulation was first introduced by Dafalias and Herrmann[10] for isotropic clays. The main features of the new model are:

(i) Combined use of radial and deviatoric mapping rules to define the loading surface, and the use of an apparent normal consolidation line for sands. During hydrostatic loading, the volumetric plastic strains are captured by means of the radial mapping rule.

(ii) Use of a non-associated flow rule where the ratio of the rates of volumetric plastic strain to deviatoric plastic strain (plastic dilatancy rate) is a function only of the ratio of deviatoric to mean effective stresses.

(iii) Adoptions of a bi-linear critical state line the plane of the void ratio versus logarithm of mean effective stress. This feature was introduced by Been et al to support a reduced slope of the critical state line in the high void ratio range for sands.

(iv)Inclusion of a sub-elliptic, or super-elliptic, segment in the plastic dilatancy surface for stress ratios less than critical.

(v) Use of elliptic segments in the deviatoric plane.

(vi) Incorporation of a plastic stiffening effect for cyclic paths which repeatedly load in the same deviatoric direction by means of memorizing the maximum previous stress excursion.

(vii) Definition of 26 surfaces for whole sphere (13 independent planes for one semi-sphere are identical to another semi-sphere's planes) to pursue plasticity individually. These planes provide an anisotropic behavior to model; also, they introduce different plasticity on each surface which is active during the given stress paths. Therefore, failure of all planes is not compulsory as failure in each plane relates to the stress/strain levels on this plane.

Details of each feature are completely described in three-dimensional space. After introducing the effective stress and strain vectors and the normal and shear stresses on each plane, the governing equations for bounding-surface plasticity are implemented. The following are subsequently defined: first, definition of planes, their local axes and the bounding surface for each plane; then, the dependence of the critical state line on the void ratio together with the apparent normal consolidation line and rebound line for each plane. The loading surface for each plane, next, is described; moreover the plastic strain rate direction, and finally, the bounding and additive plastic moduli for each plane are explained. It is demonstrated that the proposed model can culminate in precise and accurate results over a wide range of void ratios and confinement pressures for soils.

2. Definition of planes upon the new coordinates

To satisfy conditions of applicability of the framework from the engineering viewpoint, and also to reduce the extremely high computational costs, a limited number of necessary and sufficient sampling planes are considered. The choice of 13 independent planes (Figure1) for the solution of any three dimensional problem based on getting a good distribution of plastic deformation through the media and avoiding huge computing time is a fair number. The orientation of the sampling planes as given by their direction cosines of normal axis and the weight coefficients for numerical integration rule are given in fist three and the last rows of Table 1. The coefficients W_i choosing any number of sampling points, are simply calculated based on Gauss Quadrature numerical integration rule.

A coordinate system has been employed for each plane in such manner that one axis is perpendicular to the plane and the other two are laid on the plane. Plastic shear strain increments on each plane is considered as two component vectors on defined coordinate axes of plane. The presented W_i are acceptable for a first order tensor. They must be corrected for a second order tensor like stress or strain distribution over the surface of sphere. They must be multiplied by the ratio of area for each sampling plane on sphere.

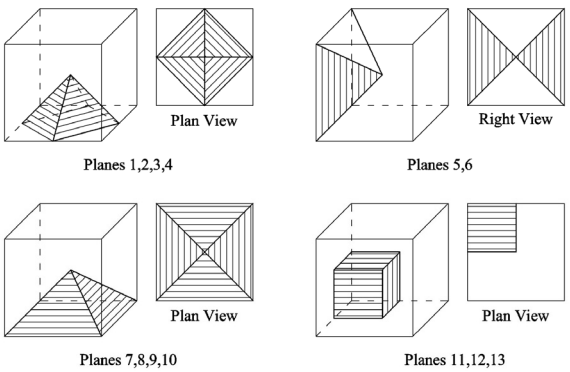

Fig. 1. Definition of 13 planes

Table 1. Cosines of normal axis and the weight coefficients for numerical integration

Plane No		1	2	3	4	5	6	7	8	9	10	11	12	13
NORMAL AXIS	l_i	$\frac{\sqrt{3}}{3}$	$\frac{\sqrt{3}}{3}$	$-\frac{\sqrt{3}}{3}$	$-\frac{\sqrt{3}}{3}$	$\frac{\sqrt{2}}{2}$	$-\frac{\sqrt{2}}{2}$	$\frac{\sqrt{2}}{2}$	$-\frac{\sqrt{2}}{2}$	0	0	1	0	0
	m_i	$\frac{\sqrt{3}}{3}$	$-\frac{\sqrt{3}}{3}$	$\frac{\sqrt{3}}{3}$	$-\frac{\sqrt{3}}{3}$	$\frac{\sqrt{2}}{2}$	$\frac{\sqrt{2}}{2}$	0	0	$-\frac{\sqrt{2}}{2}$	$\frac{\sqrt{2}}{2}$	0	1	0
	n_I	$\frac{\sqrt{3}}{3}$	$\frac{\sqrt{3}}{3}$	$\frac{\sqrt{3}}{3}$	$\frac{\sqrt{3}}{3}$	0	0	$\frac{\sqrt{2}}{2}$	$\frac{\sqrt{2}}{2}$	$\frac{\sqrt{2}}{2}$	$\frac{\sqrt{2}}{2}$	0	0	1
W_i		$\frac{27}{840}$	$\frac{27}{840}$	$\frac{27}{840}$	$\frac{27}{840}$	$\frac{32}{840}$	$\frac{32}{840}$	$\frac{32}{840}$	$\frac{32}{840}$	$\frac{32}{840}$	$\frac{32}{840}$	$\frac{40}{840}$	$\frac{40}{840}$	$\frac{40}{840}$

3. Stress and strain vectors

In all that follows { } denotes a 9-element column vector and [ ] a matrix. The superscript T indicates the transposed array. A superposed dot indicates the rate, $u(\ )$ is the Heaviside step function ($u(x>0)$=1and | | $u(x\leq 0)$=0), < > are the Macaulay brackets ($x.=u(x).x$) and refers to the norm. Following this notation |{ }| is the length of a vector whereas {| | } represents a Unit vector ({| | }={ }/|{ }|). A comma followed by a subscripted variable implies the partial derivative with respect to that variable. Bars over the stress quantities refer to points on the bounding surface (or the yield surface in conventional plasticity theory). The effective stress vector, the strain vector, the vector equivalent of the Kronecker's delta tensor are defined as

$$\begin{aligned}\{\varepsilon\}&=\{\varepsilon_{11}\ \ \varepsilon_{22}\ \ \varepsilon_{33}\ \ \varepsilon_{12}\ \ \varepsilon_{21}\ \ \varepsilon_{13}\ \ \varepsilon_{31}\ \ \varepsilon_{23}\ \ \varepsilon_{32}\}^T\\ \{\sigma\}&=\{\sigma_{11}\ \ \sigma_{22}\ \ \sigma_{33}\ \ \sigma_{12}\ \ \sigma_{21}\ \ \sigma_{13}\ \ \sigma_{31}\ \ \sigma_{23}\ \ \sigma_{32}\}^T\\ \{\delta\}&=\{1\ \ 1\ \ 1\ \ 0\ \ 0\ \ 0\ \ 0\ \ 0\ \ 0\}^T\end{aligned} \tag{1}$$

The stress vector is transferred on all planes to establish the plasticity of each one. These transfers are done by multiplying related transitive matrixes which are derived from their direction cosines. There are three stress components, first one is normal σ_n and others τ_1 and τ_2 are tangential, on each plane.

$$\begin{Bmatrix}\tau_1\\ \tau_2\\ \sigma_n\end{Bmatrix}_i=[T_i]\cdot\{\sigma\},\quad \tau=\sqrt{\tau_1^2+\tau_2^2} \tag{2}$$

$[T_i]$ is the transitive matrix of plane and i defined as:

$$[T_i]=\begin{bmatrix}L_{x_i'x} & L_{x_i'y} & L_{x_i'z}\\ L_{y_i'x} & L_{y_i'y} & L_{y_i'z}\\ L_{z_i'x} & L_{z_i'y} & L_{z_i'z}\end{bmatrix}\cdot\begin{bmatrix}l_i & 0 & 0 & m_i & 0 & n_i & 0 & 0 & 0\\ 0 & m_i & 0 & 0 & l_i & 0 & 0 & n_i & 0\\ 0 & 0 & n_i & 0 & 0 & 0 & l_i & 0 & m_i\end{bmatrix} \tag{3}$$

Based on description of local axes, and also the relations for transition of stress tensor to an arbitrary plane, we must multiply the transferred matrix by a rotation matrix to be presented in our local axes on each plane. Therefore, L is the rotation matrix, and x'_i , y'_i and z'_i are local axes of plane i and

$$\begin{aligned}S_{x_i}&=l_i\cdot\sigma_{11}+m_i\cdot\sigma_{12}+n_i\cdot\sigma_{13}\\ S_{y_i}&=l_i\cdot\sigma_{21}+m_i\cdot\sigma_{22}+n_i\cdot\sigma_{23}\\ S_{z_i}&=l_i\cdot\sigma_{31}+m_i\cdot\sigma_{32}+n_i\cdot\sigma_{33}\end{aligned} \tag{4}$$

S_{x_i} , S_{y_i} and S_{z_i} are stress component of plane i in global directions. Then, the derivatives of σ_n and τ are:

$$\sigma_{n,\sigma_i}=\begin{Bmatrix}l_i\cdot l_i\\ m_i\cdot m_i\\ n_i\cdot n_i\\ m_i\cdot l_i\\ m_i\cdot l_i\\ n_i\cdot l_i\\ n_i\cdot l_i\\ n_i\cdot m_i\\ n_i\cdot m_i\end{Bmatrix},\quad \tau_{,\sigma_i}=\left(\frac{1}{\tau}\right)\cdot\begin{Bmatrix}S_{x_i}\cdot l_i-\sigma_n\cdot l_i^2\\ S_{y_i}\cdot m_i-\sigma_n\cdot m_i^2\\ S_{z_i}\cdot n_i-\sigma_n\cdot n_i^2\\ S_{x_i}\cdot m_i-\sigma_n\cdot m_i\cdot l_i\\ S_{y_i}\cdot l_i-\sigma_n\cdot m_i\cdot l_i\\ S_{x_i}\cdot n_i-\sigma_n\cdot n_i\cdot l_i\\ S_{z_i}\cdot l_i-\sigma_n\cdot n_i\cdot l_i\\ S_{y_i}\cdot n_i-\sigma_n\cdot n_i\cdot m\\ S_{z_i}\cdot m_i-\sigma_n\cdot n_i\cdot m_i\end{Bmatrix} \tag{5}$$

In the relations related to different planes, stress components obtained from planes are not always equal to the projection of the stress tensor, and only they are equivalent in the unique condition [19]. However, generally the stress components on each plane are independent. It suffices to say that this deficiency does not produce significant error which can be omitted by calibration. The best way to avoid this problem is using virtual work rule [20-22]. Also, stress ratio of each plane defined as follows

$$\zeta=\frac{\tau}{\sigma_n} \tag{6}$$

3. Bounding surface plasticity

The plasticity of this model is very similar to the model presented by Crouch et al. [12], and follows conventional elastoplasticity expressions except some differences. A comprehensive description is given by Crouch; only the key expression regarding differences will, therefore, be presented here. The strain rate is sum of elastic and plastic components:

$$\{\dot{\varepsilon}\}=\{\dot{\varepsilon}^e\}+\{\dot{\varepsilon}^p\} \tag{7}$$

The superscripts e and p refer to the elastic and plastic parts. The recent relation can be presented as:

$$\begin{aligned}\{\dot{\varepsilon}\}&=[C^e]_T\cdot\{\dot{\sigma}\}+[C^p]_T\cdot\{\dot{\sigma}\}\\ [C^{ep}]_T&=[C^e]_T+[C^p]_T\end{aligned} \tag{8}$$

$[C^e]$, $[C^p]$ and $[C^{ep}]$ are compliance elasticity, plasticity, and elastic-plasticity matrices. For each plane:

$$[C^e]_i=\frac{1}{2G_i}[I]+\left(\frac{1}{9K_i}-\frac{1}{6G_i}\right)\cdot\{\delta\}\cdot\{\delta\}^T,\quad [C^p]_i=\frac{1}{H_i}\{Q\}_i\cdot\{P\}_i^T \tag{9}$$

$[C^e]_T$ and $[C^p]_T$ are obtained from following relation based on accumulating quotas of planes:

$$\begin{aligned}[C^p]_T&=8\pi\cdot\sum_{i=1}^{13}w_i\cdot[C^p]_i\\ [C^e]_T&=8\pi\cdot\sum_{i=1}^{13}w_i\cdot[C^e]_i\end{aligned} \tag{10}$$

On the grounds that the elastic dominion is small in soils, the elasticity parameters (Bulk and shear modules) in this model comply with the average of principal stresses, and also to avoid extra calculations, in the multi-laminate model elastic behavior is considered as isotropic one for all planes. In other words, the $[C^e]$ can be present only for the main point; thus, only the plastic behavior of the material (i.e.$[C^p]_T$) comes from numerical integration of the plastic treatment of planes (i.e. $[C^p]_T$):

$$[C^{ep}]_T=[C^e]_T+[C^p]_T \tag{11}$$

For each plane, the model needs to define four surfaces in effective stress space (i) the failure surface to define the critical-stress state. (ii) The bounding surface , to record the limit of previous loading, to help construct the loading surface and to determine the bounding plastic modulus $\bar{H}$. (iii) The loading surface f, to determine the direction of

plastic loading $\{Q\}$(which is also used to determine the direction of the deviatoric plastic strain rate) and the additive plastic modulus H_f . (iv) The plastic dilatancy surface g, (similar to a plastic potential surface) which determines the ratio of the volumetric to deviatoric plastic strain rates.

4. Failure surface

Although in the main model (presented by Crouch et al [12]) the deviatoric sections of the failure surface are assumed as elliptic form, in the multi-laminate model failure surface is supposed as Drucker-Prager conical form. The meridional sections are, however, specified by critical effective stress ratio ζ_{cr} , the slop of critical state line in σ_n-τ -plane. This parameter treated as a requisite material property, and separates the hardening and softening regions on the bounding surface.

5. Bounding surface

Three segments are constructed meridional sections of the isotropic bounding surface (i) a compressive ellipse, (ii) a hyperbola and (iii) a tensile ellipse (Figure 2). This form was originally proposed by Dafalias and Herrmann [10]. The compressive elliptic part lies in $\sigma_{n_1} \le \sigma_n \le \sigma_{n_0}$ region where $\sigma_{n_1} = \sigma_{n_0}/R$. R is a material constant $(1 \le R < \infty)$. σ_{n0} varies as a function of the volumetric plastic strain and defines the size of bounding surface. The compressive ellipse meets the normal stress axis perpendicularly. The equation of the first part is given as

$$F = \bar{\tau} - \frac{N \cdot \sigma_{n_0}}{R}\sqrt{\left(1-\left(\frac{\left(R\bar{\sigma}_n/\sigma_{n_0}\right)-1}{R-1}\right)^2\right)} = 0 \tag{12}$$

N is slope of the line which passes from common tangent point of ellipse and hyperbola. The common tangent is parallel to normal stress axis. The hyperbola is located in $\sigma_{n_2} < \sigma_n < \sigma_{n_1}$ region and defined as

$$F = \bar{\tau} - \frac{N \cdot \sigma_{n_0}}{R}\left(1+\frac{AR}{N}-\sqrt{\left(\left(1-\frac{R\bar{\sigma}_n}{\sigma_{n_0}}\right)^2+\left(\frac{AR}{N}\right)^2\right)}\right) = 0 \tag{13}$$

$A \cdot \sigma_{n_0}$ manipulates the gap between N-line and the asymptote to the hyperbolic segment, which is parallel to the N-line. The last part is a tensile ellipse situated in $\sigma_{n_3} \le \sigma_n \le \sigma_{n_2}$ where $\sigma_{n_3} = T \cdot \sigma_{n_0}$, and $\sigma_{n_2} = D \cdot \sigma_{n_0}$, and it is proposed as

$$F = \bar{\tau} - \tau_r\sqrt{\left(1-\left(1-\frac{\bar{\sigma}_n - T\sigma_{n_0}}{\sigma_{n_r}}\right)^2\right)} = 0 \tag{14}$$

$$\sigma_{n_r} = \frac{\left(\mathrm{D}\sigma_{n_0}/R\right)+\sigma_{n_0}\left(\Psi/\tau_2\right)\left(T^2-\left(\mathrm{D}/R\right)^2\right)}{1+2\sigma_{n_0}\left(\Psi/\tau_2\right)\left(T-\left(\mathrm{D}/R\right)\right)} \tag{15}$$

$$\tau_{\mathrm{r}} = \frac{\tau_2}{\sqrt{\left(1-\left(1-\frac{\left(\mathrm{D}\sigma_{n_0}/R\right)-T\sigma_{n_0}}{\sigma_{n_r}}\right)^2\right)}} \tag{16}$$

$$\Psi = \frac{N \cdot (1-D)}{\sqrt{\left((1-D)^2+(\mathrm{AR}/N)^2\right)}} \tag{17}$$

$$\mathrm{J}_2 = \frac{N \cdot \sigma_{n_0}}{R}\left(1+\frac{AR}{N}-\sqrt{\left((1-D)^2+(\mathrm{AR}/N)^2\right)}\right) \tag{18}$$

D is zero in this paper; namely, $\sigma_{n_2} = 0$. Moreover, the length of tensile cut-off is defined by σ_{n_2} . When $D=0$, T must lie in $-J_2/2\Psi\sigma_{n_0} \le T \le 0$ (the average amount of this range is recommended).

6. Critical state line, Normal consolidation line and rebound lines

In this model, the critical state, normal consolidation, and rebound lines are defined similar to what Crouch et al. [12] defined by the exception that here the space is e-$Ln\sigma_n$ instead of e-$LnI/3$. Finally, the passing line from intersection of compressive ellipse, and hyperbola segments is obtained as:

$$N = \frac{A-\zeta_{cr}\left(\frac{\sigma_{cr}}{\sigma_{n_0}}\right)-\sqrt{\left(\left(\zeta_{cr}\cdot\left(\frac{\sigma_{cr}}{\sigma_{n_0}}\right)-A\right)^2-\zeta_{cr}\cdot R\cdot\left(\frac{\sigma_{cr}}{\sigma_{n_0}}\right)^2\left(R\cdot\left(\frac{\sigma_{cr}}{\sigma_{n_0}}\right)-2\right)\left(2A-\zeta_{cr}\cdot\left(\frac{\sigma_{cr}}{\sigma_{n_0}}\right)\right)\right)}}{\left(\frac{\sigma_{cr}}{\sigma_{n_0}}\right)\cdot\left(R\cdot\left(\frac{\sigma_{cr}}{\sigma_{n_0}}\right)-2\right)} \tag{19}$$

7. Hardening/Softening equation

The most crucial hardening/softening parameter is $\dot{\sigma}_{n_0}$ which defines the size of bounding surface (the intersection of compressive ellipse with normal stress axis). Variation in the amount of this parameter is a function of volumetric plastic strain as follows:

$$\dot{k} = \dot{\sigma}_{n_0} = \frac{\left\langle \sigma_{n_0} - \sigma_l \right\rangle + \sigma_l}{\lambda - \kappa}(1+e_{in})\cdot\dot{\varepsilon}_v^p \tag{20}$$

Moreover, elastic behavior of the model is not linear, and is a function of confinement pressure. As said, elastic behavior is not transferred to planes, so the Bulk modulus complies from the hyper elastic formulation:

$$K = \frac{(1+e_{in})\cdot(\langle P-\sigma_l\rangle+\sigma_l)}{\kappa} \tag{21}$$

p and σ_l are the average amount of principal stresses at the point, and model constant, respectively. σ_l represents a limitation that there is no effect on bulk and shear modules when is lower than it. By assuming constant Poisson's ratio tangent shear modulus can be defined as:

$$G = \frac{1.5K(1-2\nu)}{1+\nu} \tag{22}$$

8. Loading surface

The model introduces an innovative approach to define the loading surface f by using deviatoric and radial mapping rules. This surface always passes through the stress point and by defining an image point on the bounding surface the similarity

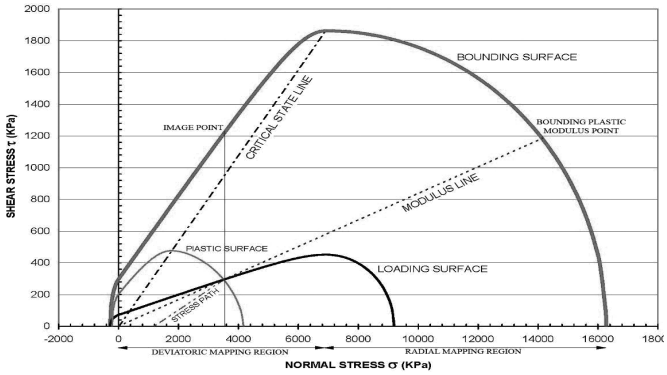

Fig. 2. Definition of the different surfaces in $\tau-\sigma$ space

ratio can be determined. The radial mapping rule is applied for the compressive ellipse part where the projection centre located at $C\sigma_{n0}$ on the σ_n axis. *C* assumes the value *1/R* in the following. When $\sigma<\sigma_{n0}/R$, the model uses deviatoric mapping rule to construct the loading surface whereas the current stress point and image point on bounding surface have the same σ_n .

If $\tau>0$ then the similarity ratio is defined as

$$\beta=\frac{\bar{\tau}}{\tau} \tag{23}$$

However, for points on the σ_n axis and $\sigma>\sigma_{n0}/R$, this ratio is determined by

$$\beta=\frac{\sigma_{n_0}\cdot\left(\frac{1}{R}-1\right)}{\frac{\sigma_{n_0}}{R}-\sigma_n} \tag{24}$$

A plastic behavior takes place during loading along σ_n axis in the radial mapping, while a completely elastic response happens during loading along σ_n axis in the deviatoric mapping region ($\tau=0$ and $\beta=\infty$). Therefore, the loading surface equation in the radial mapping region is defined by substituting for and for

$(\sigma_{n_0}/R)+\beta(\sigma_n-(\sigma_{n_0}/R))$ for $\bar{\sigma}_n$ and $\beta\tau$ for $\bar{\tau}$:

$$f=\beta\tau-\frac{N\cdot\sigma_{n_0}}{R}\sqrt{\left(1-\left(\frac{\beta(R\sigma_n/\sigma_{n_0}-1)}{R-1}\right)^2\right)}=0 \tag{25}$$

In the presented model, owing to the fact that model works with normal and shear stresses instead of stress invariants, model is able to consider the rotation of principal stresses. The related functions are, thus, specified after substituting σ_n for $\bar{\sigma}_n$ and $\beta\tau$ for $\bar{\tau}$ as follows in deviatoric mapping region instead of utilizing complicated movement rules of projection center:

$$f=\beta\tau-\frac{N\cdot\sigma_{n_0}}{R}\left(1+\frac{AR}{N}-\sqrt{\left(\left(1-\frac{R\sigma_n}{\sigma_{n_0}}\right)^2+\left(\frac{AR}{N}\right)^2\right)}\right)=0 \tag{26}$$

$$f=\beta\tau-\tau_r\sqrt{\left(1-\left(1-\frac{\sigma_n-T\sigma_{n_0}}{\sigma_{n_r}}\right)^2\right)}=0 \tag{27}$$

Now, by defining loading surface it is easy to obtain direction of plastic loading

$$\{Q\}=\frac{\{f,\sigma\}}{\left|\{f,\sigma\}\right|}=Q_v\cdot\{\delta\}+\{Q_s\} \tag{28}$$

$$\{Q\}=\frac{1}{\left|\{f,\sigma\}\right|}\cdot\left(\underbrace{f,_{\sigma_n}\cdot\{\sigma_n,\sigma\}}_{hydrostatic}+\underbrace{f,_{\tau}\cdot\{\tau,\sigma\}}_{deviatoric}\right) \tag{29}$$

The deviatoric part $\{Q_s\}$ is, then, utilized to obtain the direction of plastic strain in later sections.

9. Plastic dilatancy surface and plastic strain direction

The form of this surface is akin to bounding surface with its three segments; however, the squared terms for compressive ellipse are replaced by n_g ($2<n_g<\infty$ for super- ellipse and $1<n_g<2$ for sub-ellipse). The plastic surface, as a result, is obtained as

$$g=\tau-\frac{N_g\cdot\sigma_{n_{0g}}}{R_g}\cdot\left(1-\left(\frac{(R_g\sigma_n/\sigma_{n_{0g}}-1)}{R_g-1}\right)^{n_g}\right)^{\frac{1}{n_g}}=0 \tag{30}$$

N_g , R_g and $\sigma_{n_{0g}}$ have the identical concepts as *N, R* and σ_{n_0} for the bounding surface. Note that $\sigma_{n_{0g}}$ is scaled until the dilatancy surface passes through the current stress point.

There are three important notes about plastic dilatancy surface:

(i) The compressive ellipse meets the normal stress axis perpendicularly. This is, in this point all amounts of plastic strain are volumetric.

(ii) The common tangent of Hyperbola and Compressive ellipse segments is parallel to normal stress axis. In other words, in this point all amounts of plastic strain are deviatoric.

(iii) $N_g=\zeta_{cr}$, this means that the vertex of the plastic dilatancy surface (intersection of compressive ellipse and hyperbola) is met by critical state line, where the horizontal projection of plastic strain direction is zero; thus, all amounts of plastic strain are deviatoric.

Despite the fact that the shape of bounding surface and plastic dilatancy surface are similar [23], flow rule is non-associated, as bounding surface and loading surface are not geometrically similar by virtue of the mapping rules. Then the direction of the plastic strain rate is obtained as:

$$\{P\}=\frac{1}{\left|\{g,\sigma\}\right|}\cdot\left(g,_{\sigma_n}\cdot\{\sigma_n,\sigma\}+f,_{\tau}\cdot\{\tau,\sigma\}\right) \tag{31}$$

10. Bounding and additive plastic moduli

The bounding plastic modulus point is a point on the bounding surface and it has the same ζ with the current stress point [24]. To define this point, we can draw a line from origin to the current stress point and continue until it intersects the

bounding surface.

Knowing $\dot{\varepsilon}_v^p = \{\delta\}^T\{P\}$ and substituting equation (20) will be:

$$\dot{k} = \frac{\langle \sigma_{n_0} - \sigma_l \rangle + \sigma_l}{\lambda - \kappa}(1+e_{in})\{\delta\}^T\{P\} \tag{32}$$

And bounding plastic modulus, $\overline{H}$:

$$\frac{1}{\overline{H}} = -\frac{\left|\{F_{,\bar{\sigma}}\}\right|}{F_{,\sigma_{n_0}} \cdot \dot{k}} \tag{33}$$

By balancing the last two equations, $\overline{H}$ is obtained as

$$\overline{H} = -\frac{\left(\langle \sigma_{n_0} - \sigma_l \rangle + \sigma_l\right)\cdot(1+e_{in})}{\lambda - \kappa}\frac{F_{,n_0}}{\left|\{F_{,\bar{\sigma}}\}\right|}\{\delta\}^T\{P\} \tag{34}$$

Where $F_{,n_0}$ and $\left|\{F_{,\bar{\sigma}}\}\right|$ are calculated at the bounding plastic modulus. In addition, proximity-dependent additive plastic modulus can be defined as

$$H_f = \frac{\left(\langle \sigma_{n_0} - \sigma_l \rangle + \sigma_l\right)\cdot(1+e_{in})}{\lambda - \kappa}\frac{h}{\langle \beta/(\beta-1) - s \rangle^{n_H}}\left(\frac{\left(\langle \sigma_{n_0} - \sigma_l \rangle + \sigma_l\right)}{\sigma_{at}}\right)^{z_0} \tag{35}$$

h, s and σ_{at} are shape hardening factor, ratio of the size of elastic kernel and atmosphere pressure, respectively. Moreover, z_0 and n_H are material constants.

Generally, s defines a elastic zone enclosing the projection centre. z_0 shows the importance of a stiffer behavior for denser states, and n_H controls the rate at which the additive plastic modulus falls with respect to the proximity of the current stress point to its image point on the bounding surface.

The shape hardening parameter which has a strong effect on behavior of the model for stress paths inside the bounding surface is derived by h_1 and h_2, which are the coincident amounts of $\sigma_{n_1} = \sigma_{n_0}/R$ and $\sigma_{n_2} = 0$.

$$h = \left(h_1 - \left\langle 1 - \frac{\sigma_n R}{\sigma_{n_0}} \right\rangle \cdot (h_1 - h_2)\right)\cdot\left(1 + z_1\left\langle 1 - \left(\frac{\tau}{\max(\tau)}\right)^{Z_2}\right\rangle\right) \tag{36}$$

Where z_1 and z_2 are the material constants, and $max(\tau)$ is the maximum quantity of shear stress along the stress path.

11. Exprimental results

Figure 3 shows the volumetric strain versus axial strain drained behavior for four loose specimens e_{in}=*0.86* together with their cell pressures σ_3. The sample under the highest cell pressure undergoes considerable compaction up to 5% for ε_v, while sample under the lowest cell pressure presents a moderate dilation at 20% axial strain despite being in a loose state. Figure 4 shows the corresponding drained curves for five dense samples e_{in}=*0.86*. The significant dilation up to 12% for ε_v under low cell pressures is captured well by the model.

12. Undrained loading

The definition of effective stress for a saturated soil element is stated in macro scale and incremental form as follows [25]:

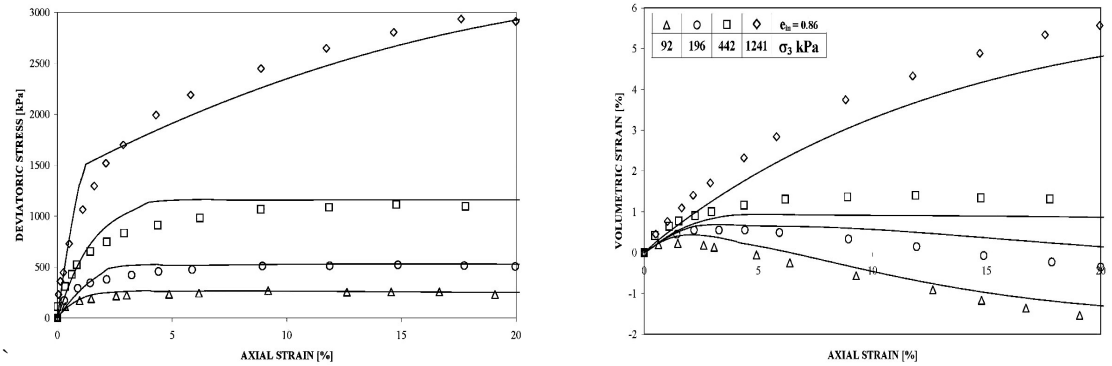

Fig. 3. Axial strain versus volumetric strain, and deviatoric stress in loose sand (e_{in}=*0.86*).

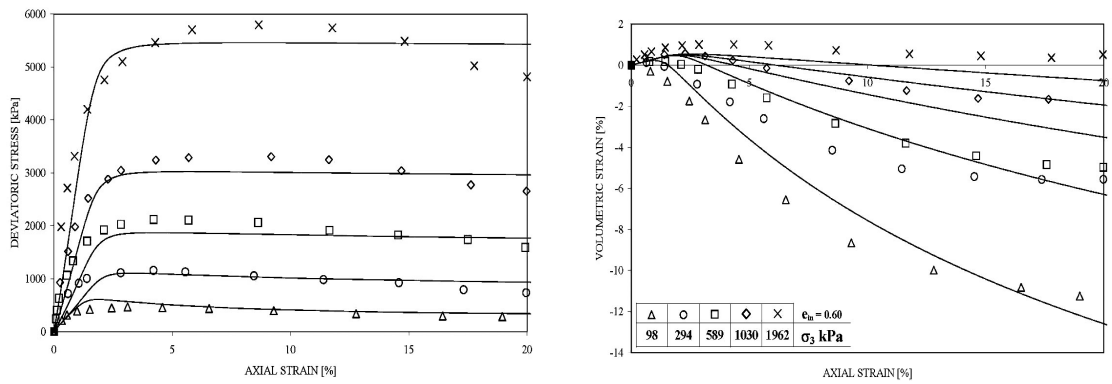

Fig. 4. Axial strain versus volumetric strain, and deviatoric stress in loose sand (e_{in}=*0.60*).

$$\{d\sigma\} = \{d\sigma'\} + \{\delta\} \cdot dU \tag{37}$$

σ and σ' are representatives of total and effective stresses vectors respectively, U is the excess pore water pressure, and d is used for representing small increments. It can also be assumed that in a fully undrained case, the skeleton volume change is approximately equal to change in the volume of pore water. Defining K_f as average bulk modulus of soil skeleton,

$$dU = K_f \cdot \{\delta\}^T \cdot \{d\varepsilon\} \tag{38}$$

$$\frac{1}{K_f} = \frac{1}{K_w} + \frac{1-v}{K_s} \tag{39}$$

K_w is bulk modulus of water and v is initial porosity. Pore water pressure increment in matrix form is written as follows:

$$dU = K_f \cdot \{\delta\}^T \cdot \{d\varepsilon\} \cdot \{\delta\} \tag{40}$$

Retaining the elastic-plastic constitutive law, it is presented as follows:

$$\{d\sigma'\} = [D^{ep}] \cdot \{d\varepsilon\} \tag{41}$$

$$\{d\sigma'\} = [D^{ep}] \cdot \{d\varepsilon\} \tag{42}$$

$[D^{ep}]$ and $[D^{ept}]$ are effective and total stress-strain matrices. Substituting equations 40, 41, and 42 in 37 simply result is:

$$[D^{ept}] = [D^{ep}] + K_f \cdot \{\delta\}^T \cdot \{\delta\} \tag{43}$$

$$[C^{ep}] = [C^e] + [C^P], \quad [D^{ep}] = [C^{ep}]^{-1} \tag{44}$$

$[C^e]$, $[C^p]$, and $[C^{ep}]$ are compliance elasticity, plasticity, and elastic-plasticity matrices. According to incremental algorithm, $[C^{ep}]$ computed in previous step can be used for current step; therefore, the solution will not remain indeterminate. Consequently, $[C^{ept}]$ can be employed to calculate strain increments upon total stress increment tensor.

The sensitivity of model prediction to the above 13 parameters are investigated and presented as following Figures.

Table. 2. Identification of parameters and their sensitivities on the model

Critical state line slope in $e-\ln(I/3)$ space	$:\lambda$
Changed value of critical state line slope in $e-\ln(I/3)$ space at e_{crk}	$:\lambda_L$
Parameter for size of boundary surface	$:A_c$
Parameter for size of boundary surface of plastic potential	$:A_{gc}$
Shape hardening parameter	$:h_{1c}$
Ratio of normal stresses boundary surface and compression and hyperbolic ellipsoid	$:R$
Poisson ratio	$:\nu$
Power in compression ellipse of plastic potential	$:n_g$
Unloading line slope	$:\kappa$
Initial void ratio	$:e_{in}$
Critical state line slope in $I-J$ space	$:\zeta_{cr_c}$
Initial mean stress	$:P_o$
Void ratio of critical state line slope in $e-\ln(I/3)$ space at e_{crk}	$:e_{cr_k}$

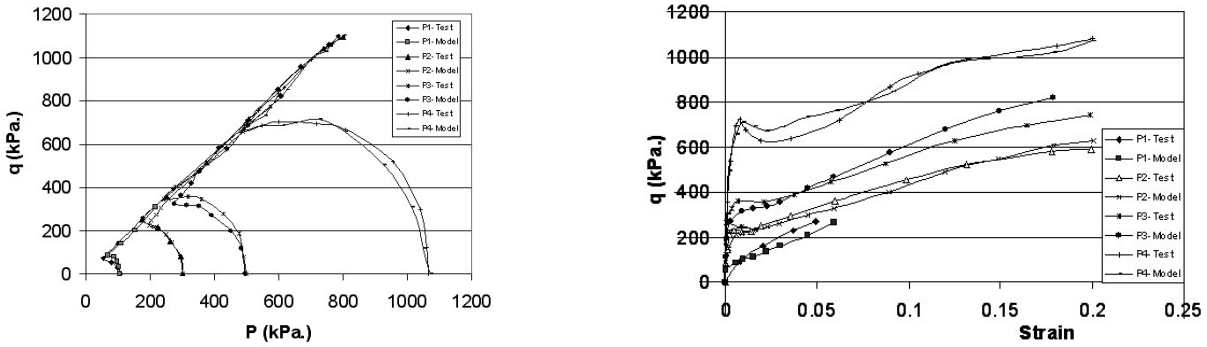

Fig. 5. Stress paths and deviatoric stress versus axial strain in loose sand.

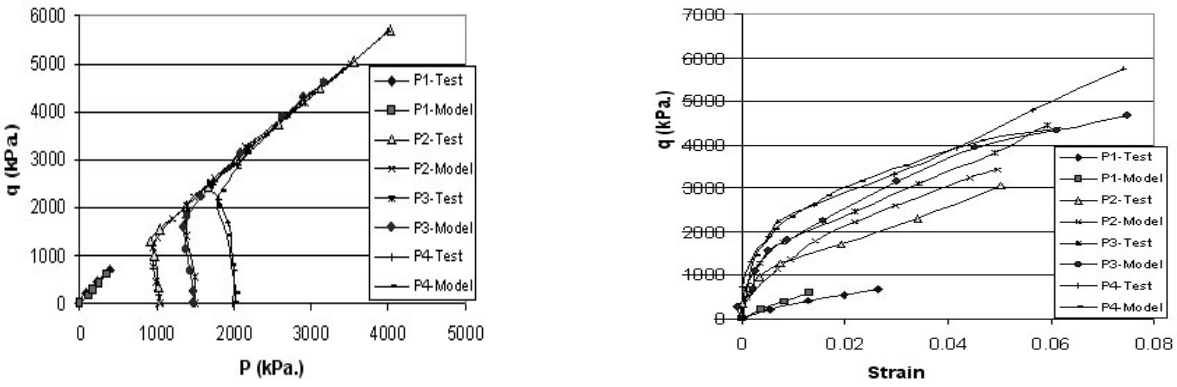

Fig. 6. Stress paths and deviatoric stress versus axial strain in stiff sand.

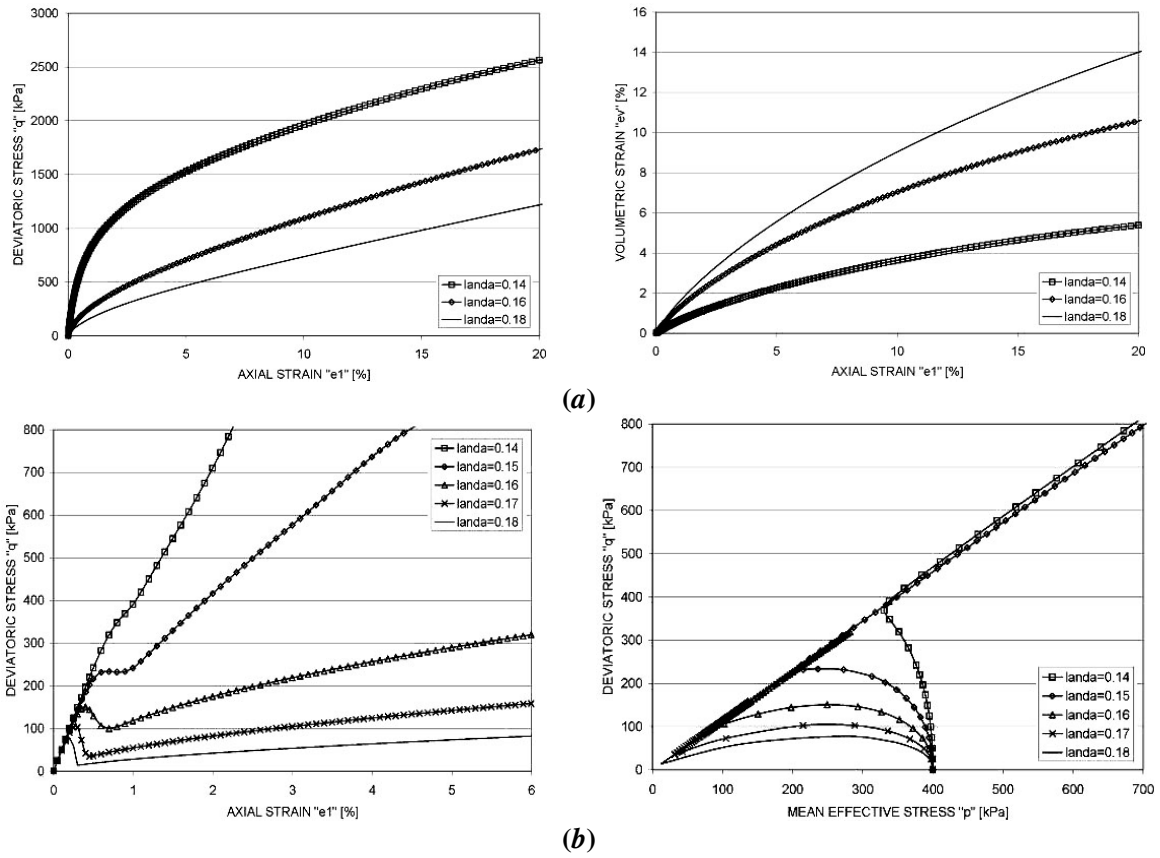

Fig. 7. The effects of parameter λ in a) Drained b) Undrained

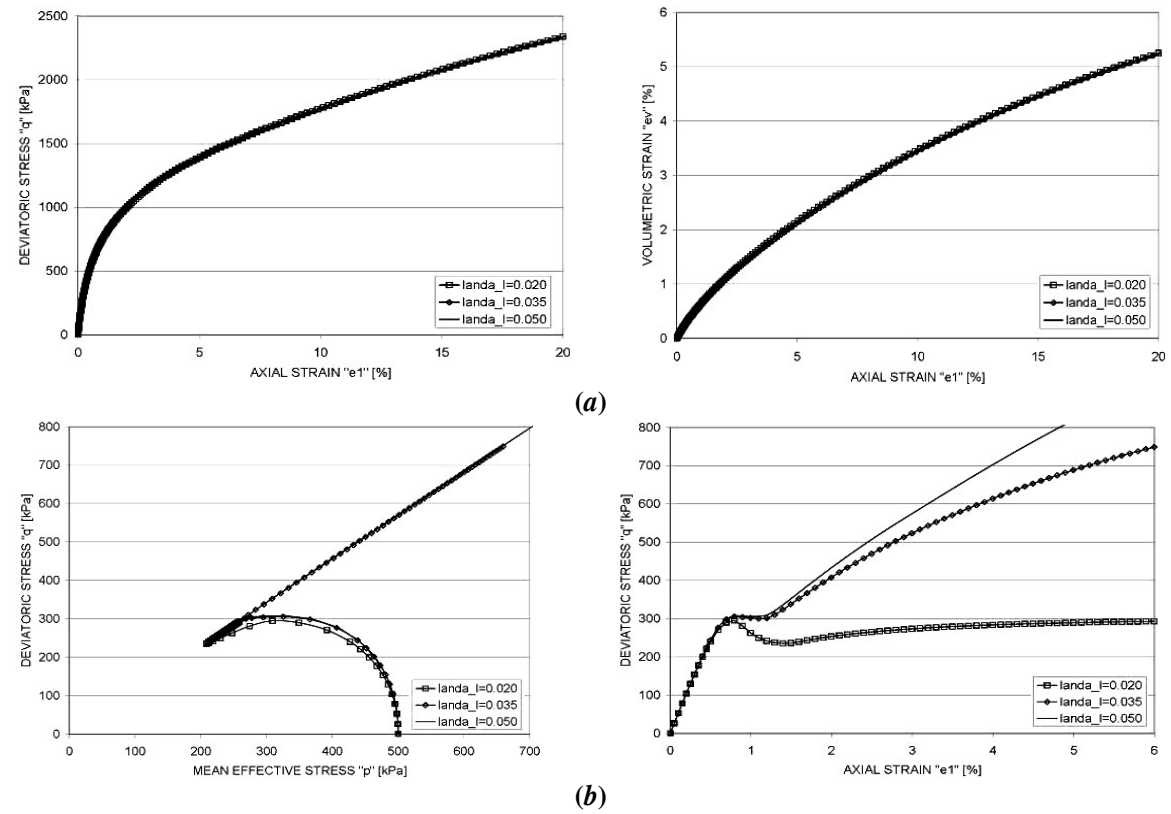

Fig. 8. The effects of parameter λ_L in a) Drained b) Undrained

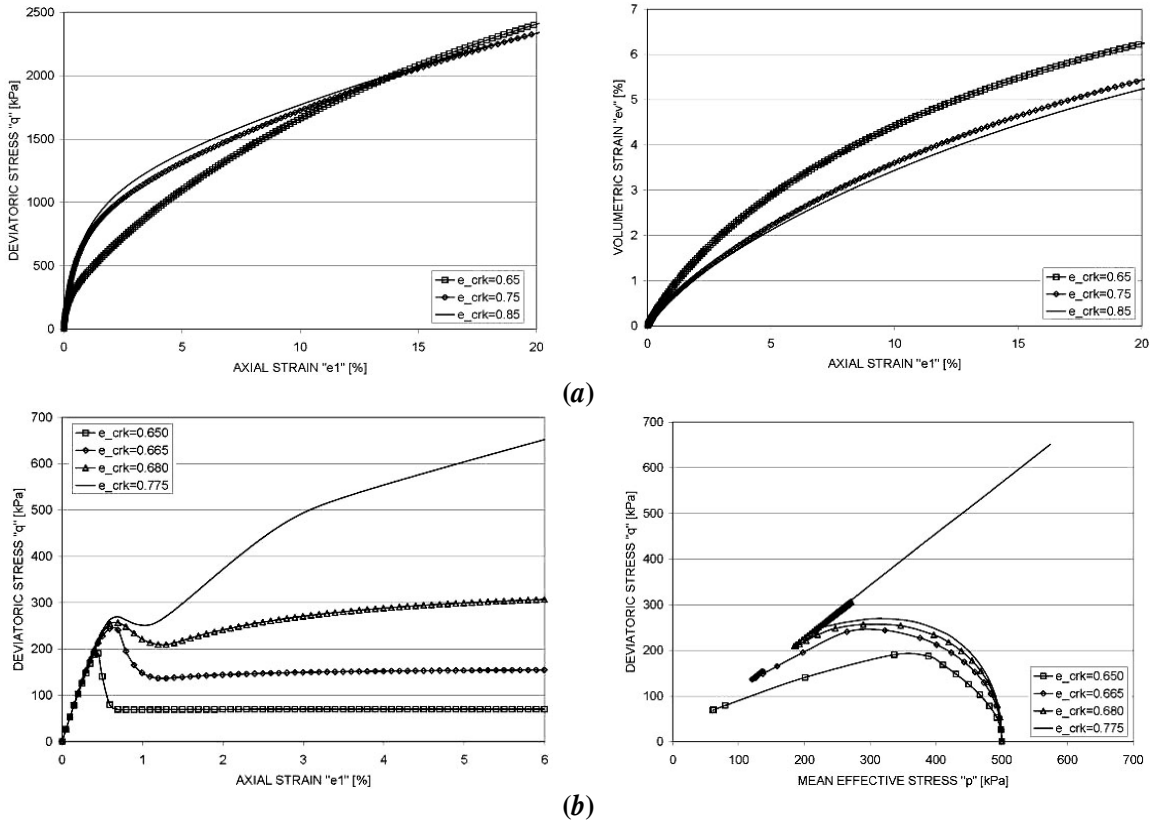

Fig. 9. The effects of parameter e_{crk} in a) Drained b) Undrained

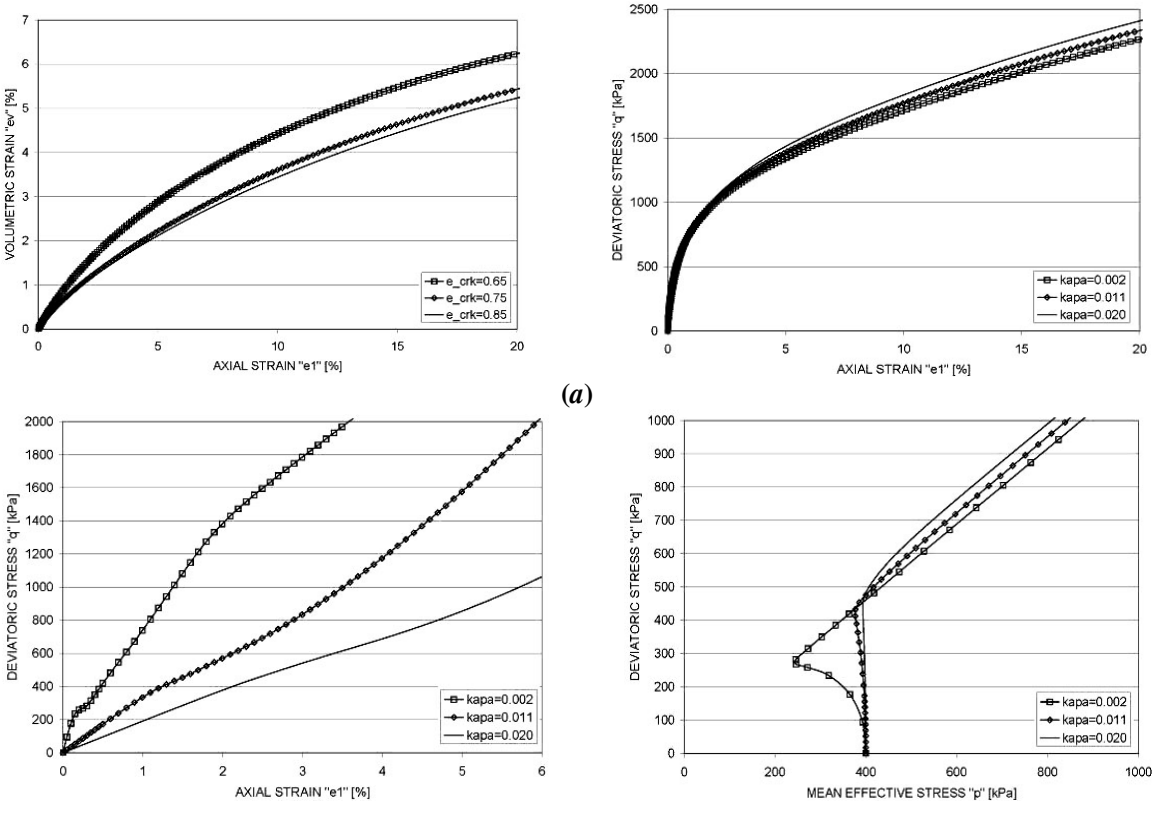

Fig. 10. The effects of parameter k in a) Drained b) Undrained

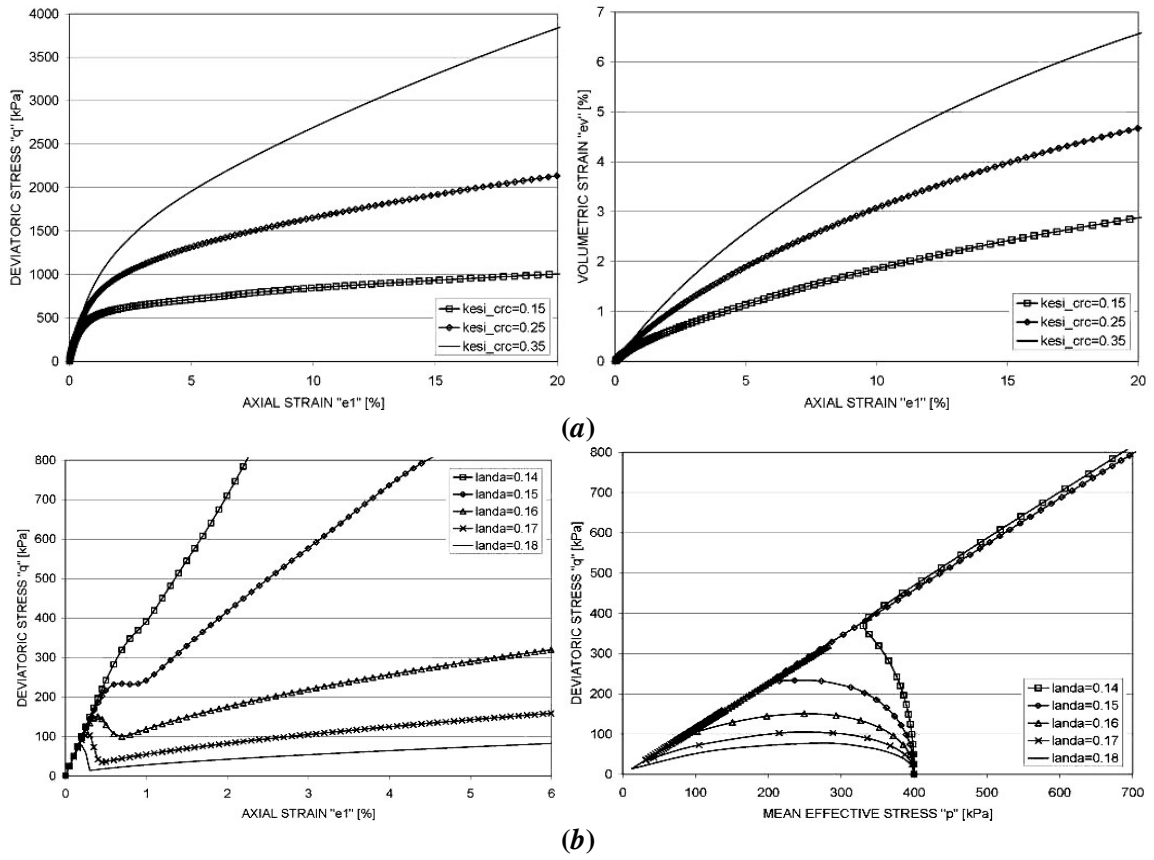

Fig. 11. The effects of parameter ζ_{rc} in a) Drained b) Undrained

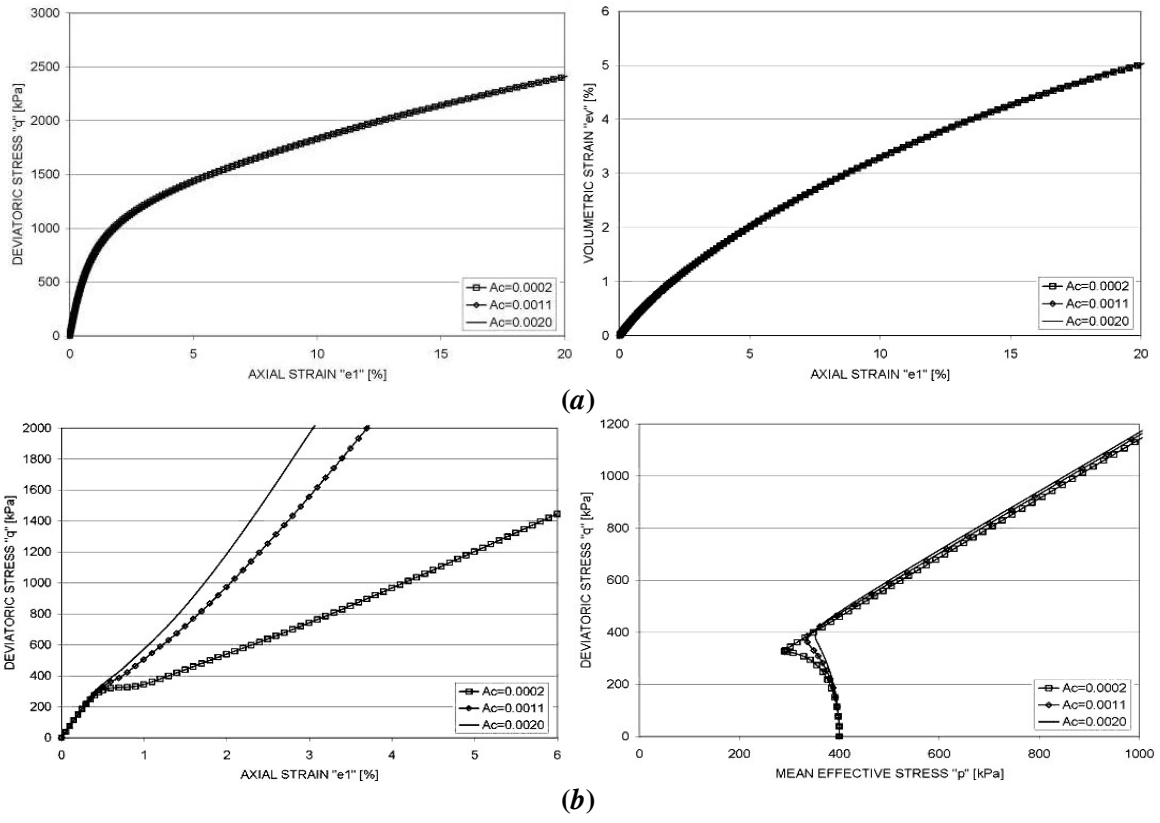

Fig. 12. The effects of parameter A_c in a) Drained b) Undrained

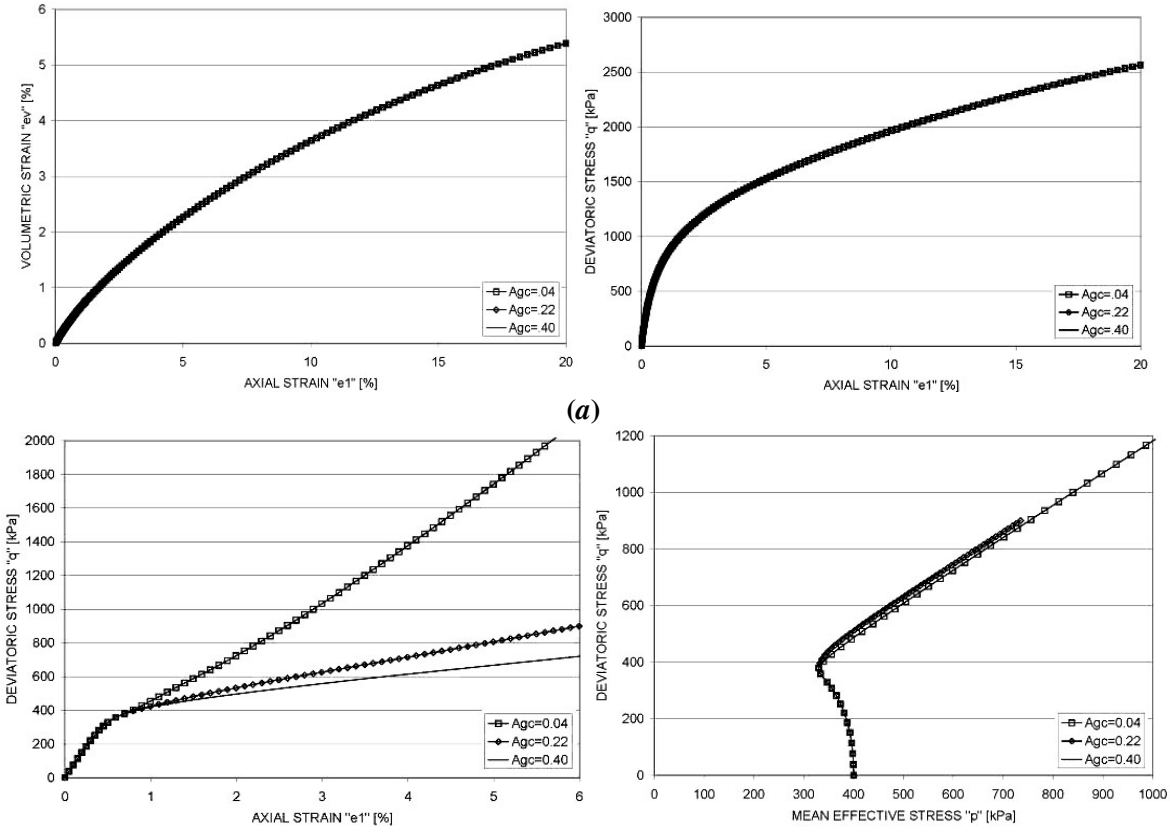

Fig. 13. The effects of parameter A_{ge} in a) Drained b) Undrained

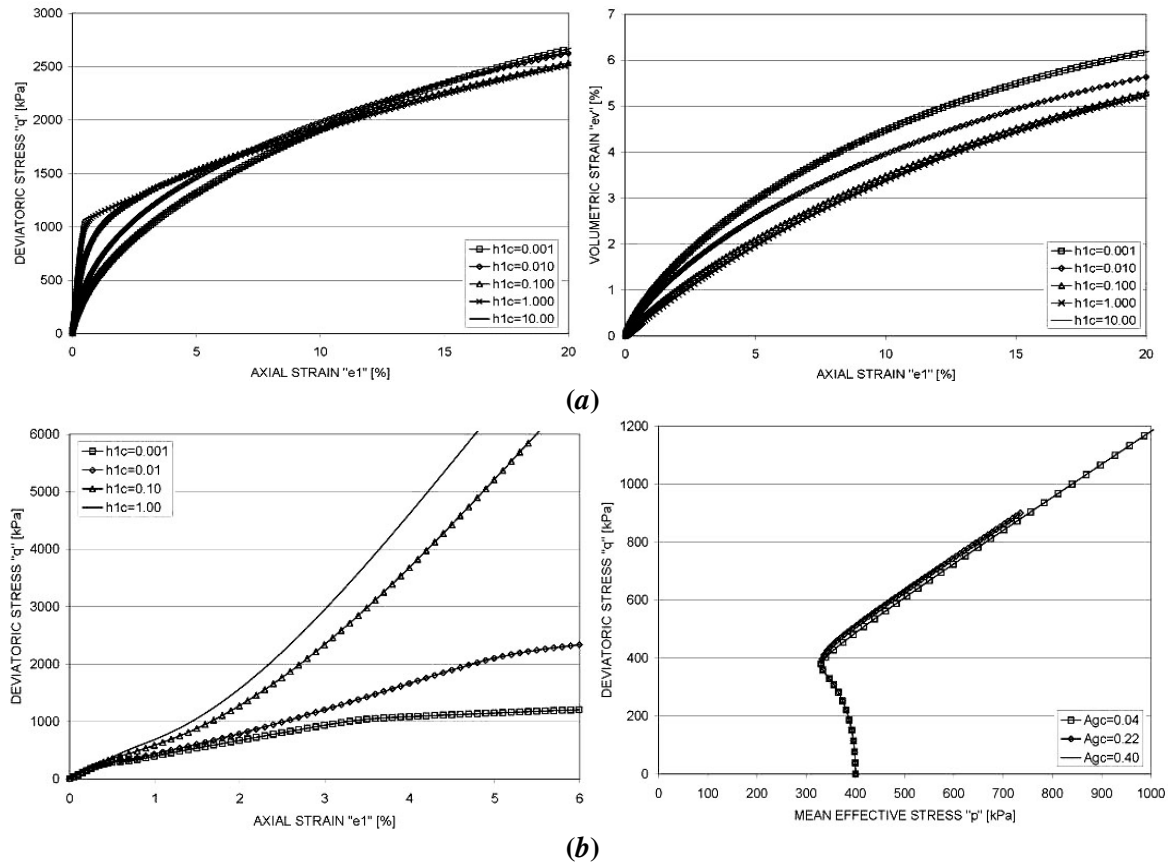

Fig. 14. The effects of parameter h_{1c} in a) Drained b) Undrained

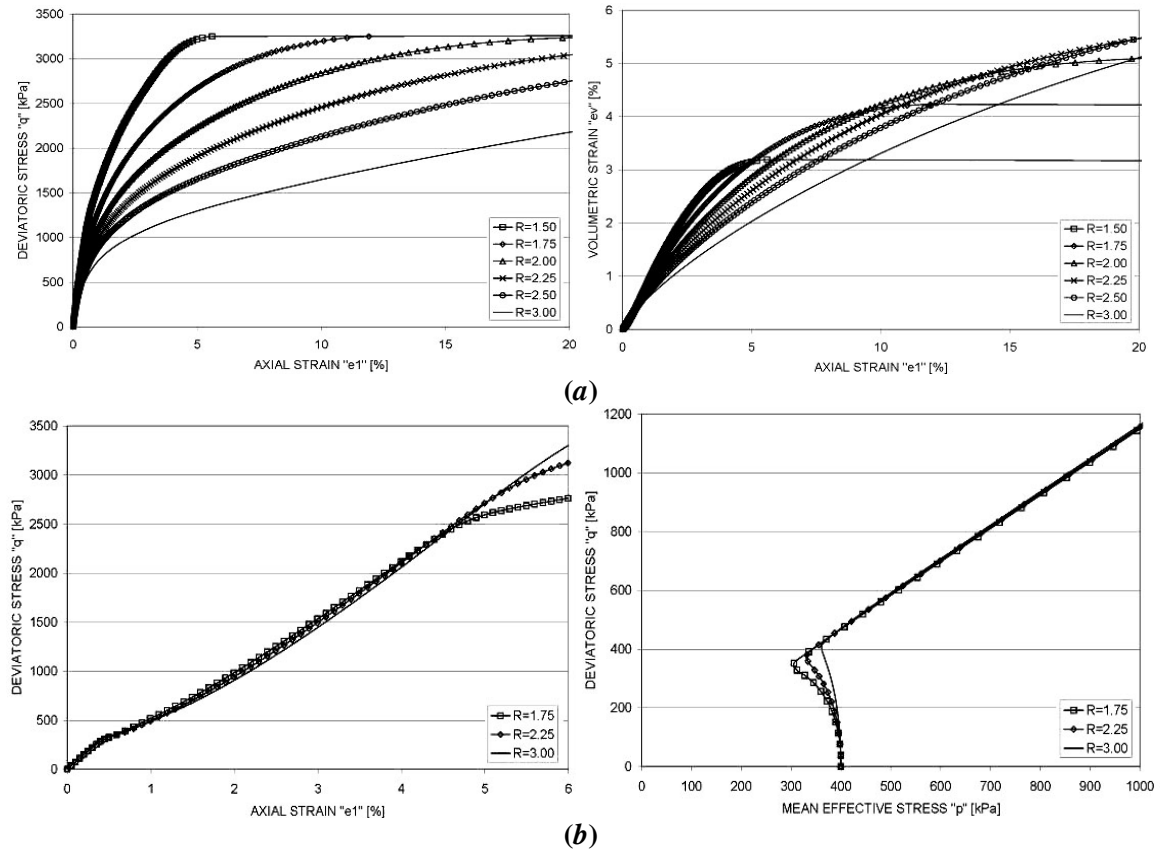

Fig. 15. The effects of parameter R in a) Drained b) Undrained

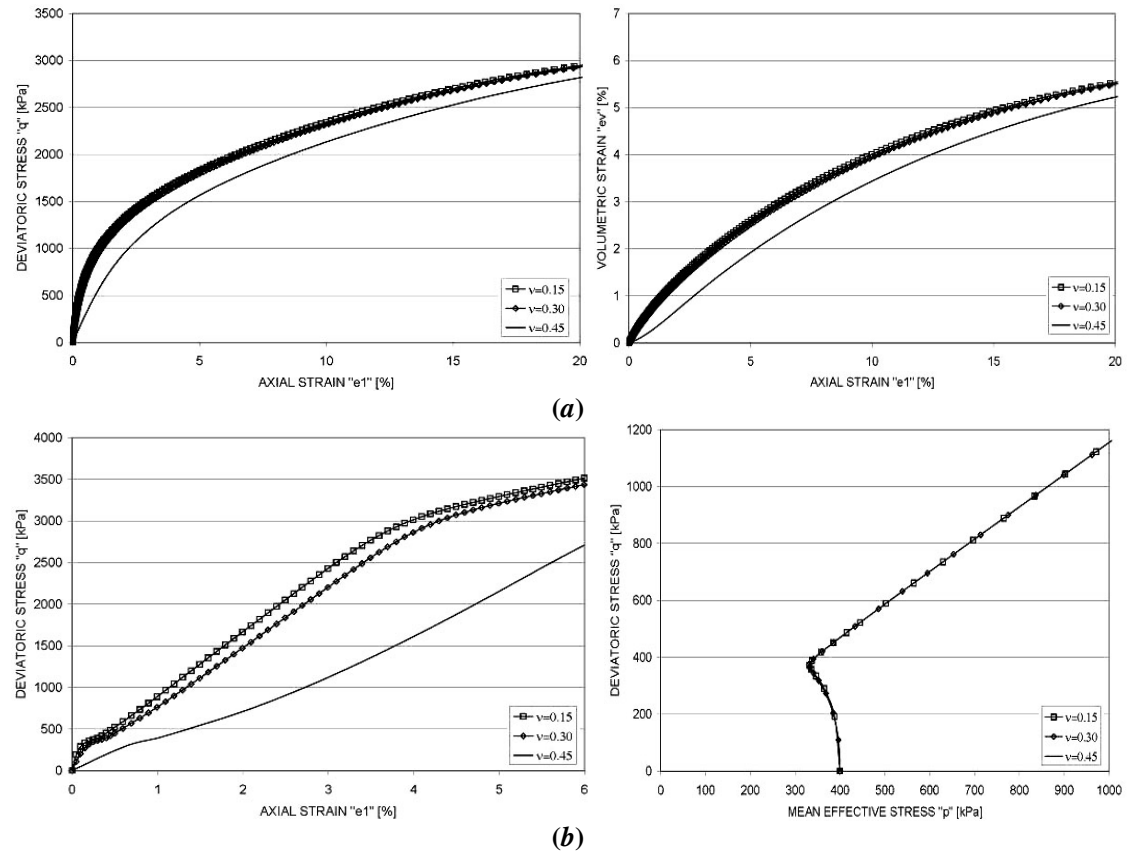

Fig. 16. The effects of parameter v in a) Drained b) Undrained

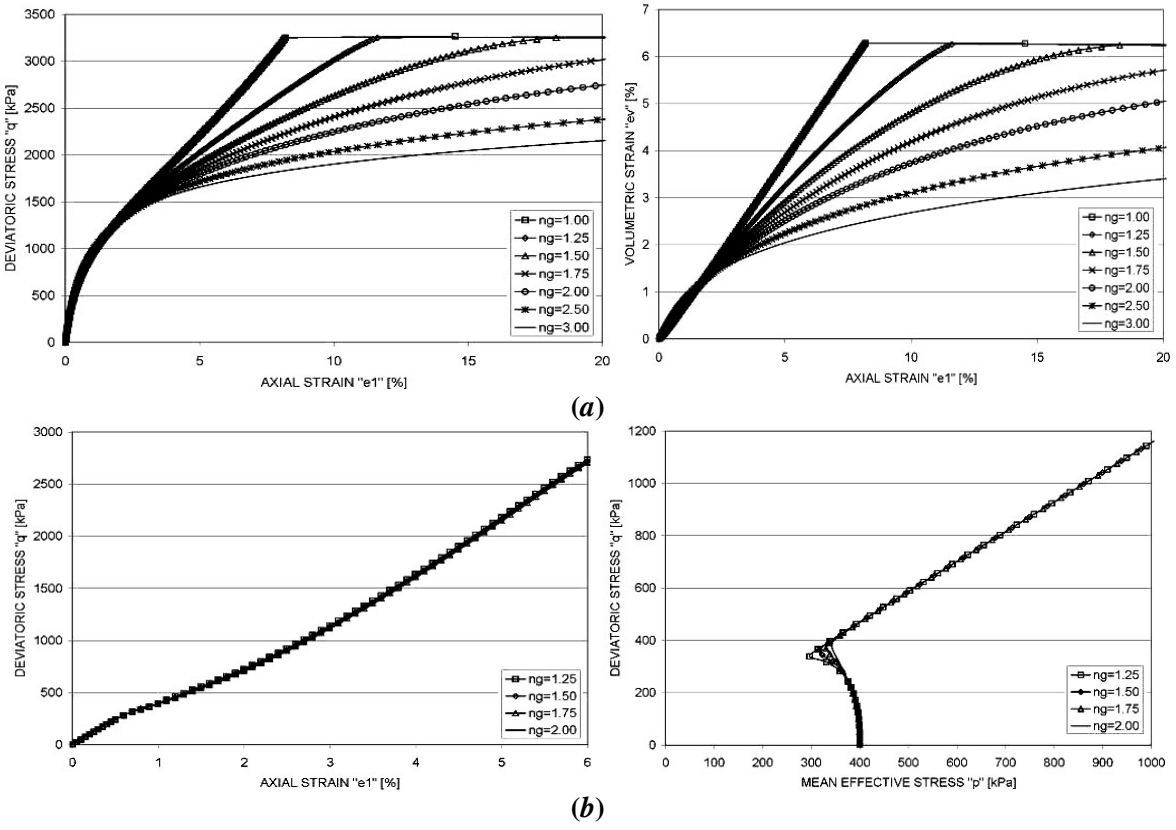

Fig. 17. The effects of parameter n_g in a) Drained b) Undrained

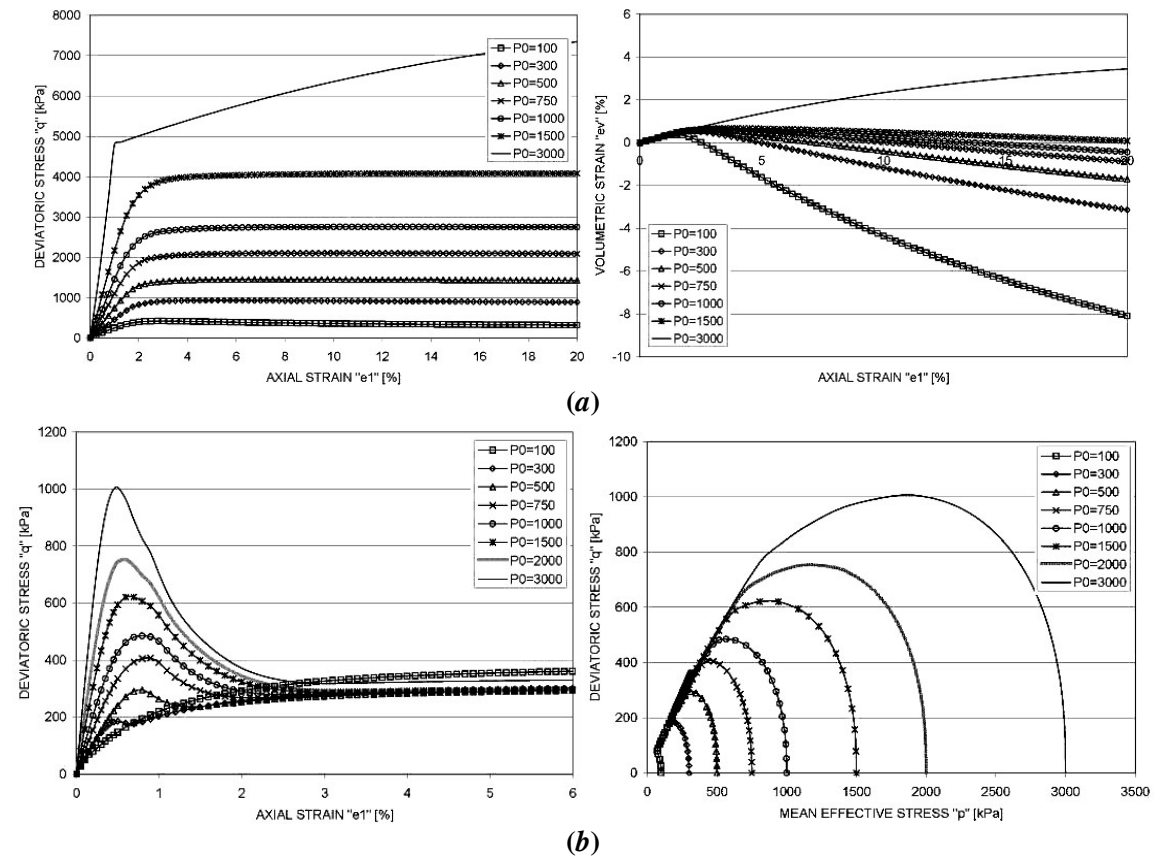

Fig. 18. The effects of parameter P_0 in a) Drained b) Undrained

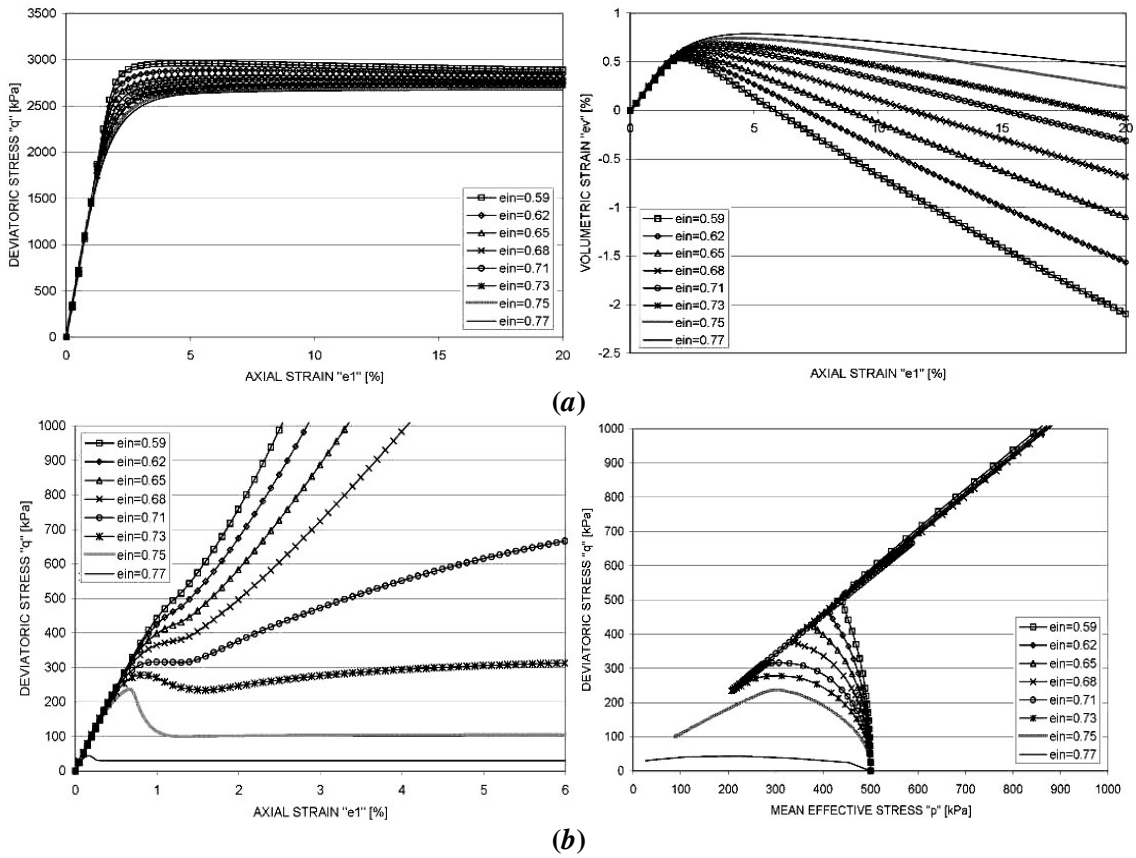

Fig. 19. The effects of parameter e_{in} in a) Drained b) Undrained

13. Conclusion

A multilaminate bounding surface model is presented which simulates drained and undrained as pre- and post-liquefaction behaviour of sand. The model permits simultaneous evaluation of triggering and post-liquefaction displacement. It directly considers the reduced stiffness, strength anisotropy, and occurrence of high pore pressure (r_u = 100%) in liquefied soils. Triggering of liquefaction is evaluated on the nearest sampling planes orientation through liquefied elements, permitting deformation of zones of liquefaction to develop with loading in a rational manner. The effects of progressive liquefaction leading to failure, including base isolation and load shedding, are directly considered.

A Multilaminate numerical algorithm is also capable to achieve a better anticipation of load inclination effects through material. In this way, the directional information and effects of applied load orientation on mechanical behavior of material are addresses and considered. Further than possibility of predicting inherent anisotropy, this rational way facilitates to the model to predict induced anisotropy and a potential to solve anisotropy of material through defining different mechanical behavior on different orientation. This is achieved by the use of a generally simplified, applicable, effective, and easily understandable relations between micro and macro scales. These relations demonstrate an easy way to handle any heterogeneous material property as well as mechanical behavior of materials.

This model is able to solve a three dimensions plasticity problem by a rather simple theory based on the phenomenological description of two dimensions plastic deformation and kinematics hardening of materials. This, is actually, achieved in such a way that the application of some difficult tasks such as induced and inherent anisotropy and rotation of principal stress and strain axes where there may be not coaxiality of them during plastic flow, to be predictable. Accordingly, the sampling plane constitutive formulations provide convenient means to classify loading events generate history rules and formulate independent evolution rules for local variables.

References

[1] Drucker, D. C., Gibson, R. E., and Henkel, D. l. (1957). "Soil mechanics and work-hardening theories of plasticity." Trans., ASCE, 122, 338-346.

[2] Roscoe, K. H., and Burland, J. B. (1968). "On the generalized stress-strain behaviour of 'wet' clay." Engineering Plasticity. J. Heymann and F. A. Leckie, eds., Cambridge University Press, Cambridge, England, 535-609.

[3] DiMaggio, F. L. and Sandler, I. S. (1971). "Material model for granular soils." J. Engr. Mech. Div., ASCE, 97(3), 935-950.

[4] Lade, P. V. (1977). "Elasto-plastic stress-strain theory for cohesionless soil with curved yield surfaces." Int. J. Solids Struct., 13, 1019-1035.

[5] Prevost, J-U. (1978). "Plasticity theory for soil stress-strain behavior." J. Engr. Mech. Div., ASCE, 104(5), 1177-1194.

[6] Mroz, Z., Norris, V. A., and Zienkiewicz, 0. C. (1981). "An anisotropic, critical state model for soils subjects to cyclic

loading." Geotechnique, London, England, 31(4), 451-469.
[7] Ghaboussi, J. and Momen, H., (1982); "Modeling and analysis of cyclic behavior of sands", G. N. Pande and O. C. Zienkiewicz (eds), Soil Mechanics-Transient and Cyclic Loads, Wiley, New York, 313-342.
[8] Dcsai, C. S., and Faruque, M. 0. (1984). "Constitutive model for (geological) materials.' I. Engr. Mech., ASCE, 110(9), 1391-1408.
[9] Poorooshasb, H. B. and Pietruszczak, S., (1985); "On yielding and flow of sand; a generalized two-surface model", Computers and Geomechanics, 1, 33-58.
[10] Dafalias, Y. F. and Herrmann, L. R.,1986, Bounding surface plasticity. II: Application to isotropic cohesive soils. In: Journal of Engineering Mechanics, 112 (12), 1263-1291.
[11] Frantziskonis, G., Desai, C. S., and Somasundaram, S. (1986). "Constitutive model for non-associative behavior." J. Engr. Mech., ASCE, 112(9), 932-946.
[12] Crouch, R. S. and Wolf, J. P., 1994, Unified 3D Critical State Bounding Surface Plasticity Model for Soils Incorporating Continuous Plastic Loading under Cyclic Paths. Part I: Constitutive relations. In:International Journal of Numerical and Analytical Methods in Geomechanics, 18, 735-758.
[13] Taylor G. I., (1938); "Plastic strain in metals", Journal of industrial metals, 62, 307-324.
[14] Batdorf S. B. and Budiansky B., (1949); "A mathematical theory of plasticity based on the concept of slip", National advisory committee for Aeronautics, T1871.
[15] Zienkiewicz, O.C., Pande G.N., (1977); "Time-dependent Multilaminate model of rocks - a numerical study of deformation and failure of rock masses", International Journal of Numerical and Analytical Methods in Geomechanics, 1, 3, 219 - 247.
[16] Pande G. N. and Piretruszczak S., (1982); "Reflecting surface model for soils", proceeding International Symposium Numerical Methods in Geomechanics, Zurich, A.A. Balkema, Rotterdam, 50-64.
[17] Pande G. N. and Sharma K. G., (1983); "Multilaminate model of clays", International Journal of Numerical and Analytical Methods in Geomechanics.
[18] Bazant Z. P. and Oh B. H., (1983); "Micro plane model for fracture analysis of concrete structures", Proceeding Symposium on the interaction of Non-nuclear munitions with structures, published by McGregor & Werner, Washington.
[19] Bazant, Z. P. and Oh, B. H.,1983. Micro plane model for fracture analysis of concrete structures. In: Proceeding Symposium on the interaction of Non-nuclear munitions with structures, published by McGregor & Werner, Washington.
[20] Hashiguchi, K. and Chen, Z.P., 1998. Elastoplastic constitutive equation of soils with the subloading surface and the rotational hardening. In: International Journal of Numerical and Analytical Methods in Geomechanics, 22, 197-227.
[21] Baziar, M.H., and Ghorbani, A., 2009, Small-Scale Model Test and Three-Dimensional Analysis of Pile-Raft Foundation on Medium-Dense Sand, International Journal of Civil Engineering, Vol.7, No.3, pp 161-170.
[22] Hassanlourad, M., Salehzadeh, H., Shahnazari, H., 2008, Dilation and Particle breakage effects on the Shear Strength of Calcareous Sands based on energy Aspects, International Journal of Civil Engineering, Vol. 6, No. 2, pp 108-120.
[23] Soltani-Jigheh, H., and Soroush, A., 2006, Post-cyclic Behavior of Compacted Clay-sand Mixtures, International Journal of Civil Engineering, Vol.4, No. 3, pp 226-244.
[24] Khoei, A.R., and Yadegari, S., and Anahid, M., 2006, Three Dimensional Modeling of Strain Localization in Cosserat Continuum Theory, International Journal of Civil Engineering, Vol.4, No. 3, pp 176-192.
[25] Soroush, A., and Koohi, Sh., 2004, Liquefaction-Induced Lateral Spreading- An Overview and Numerical Analysis, International Journal of Civil Engineering, Vol. 2, No. 4, pp 232-246.